



# Effect of interlayer dwell time on output quality in wire arc additive manufacturing of low carbon low alloy steel components

Batuhan Turgut<sup>1,2</sup> · Uğur Gürol<sup>2,3</sup> · Recep Onler<sup>1</sup>

Received: 20 November 2022 / Accepted: 23 April 2023 / Published online: 1 May 2023  
© The Author(s), under exclusive licence to Springer-Verlag London Ltd., part of Springer Nature 2023

## Abstract

Wire arc additive manufacturing (WAAM) has gained significant attention over the past decade due to its advantages, such as high productivity, cost-effectiveness, and ease of application. However, predictable WAAM of components with designed properties is still challenging due to the lack of comprehensive understanding of the process that uses considerable heat input. The interlayer dwell time is a critical process parameter in WAAM that impacts the thermal history of the manufacturing part, thereby controlling the output quality. This experimental study investigates the effect of interlayer dwell time on the microstructure and mechanical properties of low carbon low alloy steel components fabricated by WAAM. Three samples were produced by WAAM using identical process conditions by employing continuous deposition, 60 s, and 120 s dwelling after each layer deposition, respectively. The temperature profiles on both the substrate and the interlayer, hardness, yield strength, and microstructure variation were comparatively investigated. It was shown that the interlayer dwell time can significantly allow controlling the temperature fields experienced in the part, in turn, both mechanical and microstructural properties are modified. In addition, since the distance to the substrate increases with increasing built height, the thermal history and local properties of the specimens were found to be affected. Thus, a constant interlayer dwell time does not provide identical interlayer temperatures. It was found that compared to the samples without interlayer dwell time the samples with 120 s dwell time showed around 18% and 10% increased average hardness and average yield strength, respectively.

**Keywords** Additive manufacturing · Wire arc additive manufacturing · Interlayer dwelling · Hardness · Microstructure

## 1 Introduction

In recent decades, wire arc additive manufacturing (WAA) has gained and increasing attention for rapid fabrication of three-dimensional complex, large parts and components due to its high deposition rates, low cost, and ease of application and broad materials selection [1, 2]. The WAAM process uses an electrical arc and filler wires as the heat source and deposition material, respectively, to provide the desired heat input during the layer-by-layer deposition of materials. Furthermore, WAAM leverages the established welding

processes with various materials, thereby highlighting the industrial feasibility of WAAM [3]. Despite the aforementioned advantages, in-depth understanding of the WAAM process is lacking, which renders predictable fabrication of high-quality parts via WAAM challenging.

The output quality of the parts created by WAAM depends highly on their thermal history [4–6]. This heat input is pivotal for adhesion of layers in WAAM; however, it also poses inherent challenges, such as (1) the potential excessive heat accumulation would result in catastrophic interruption of the process due to structural failures, poor dimensional accuracy, and unwanted alterations of mechanical properties and microstructure [4, 7–10]; and (2) the possibility of uncontrolled thermal cycles experienced by the parts due to the conductive heat transfer to the substrate in WAAM would lead to significant anisotropy, especially when creating complex parts with a large number of layers [5, 6, 11–13]. As such, it is crucial to understand and control the thermal history-output quality relationships of the parts to fabricated by WAAM.

✉ Recep Onler  
ronler@gtu.edu.tr

<sup>1</sup> Department of Mechanical Engineering, Gebze Technical University, Gebze, 41400 Kocaeli, Turkey

<sup>2</sup> Gedik Welding Inc., Research and Development Center, Pendik, 34906 İstanbul, Turkey

<sup>3</sup> Department of Metallurgical and Materials Engineering, İstanbul Gedik University, Pendik, 34906 İstanbul, Turkey

Since WAAM process has a wide range of process parameter selections that can directly affect the thermal history-output quality relationship, many researchers focus on identifying suitable process parameter selections. For example, Müller et al. investigated the effect of heat input, interlayer temperature, and cooling rate on the mechanical properties of high-strength steel structures, and demonstrated that the microstructure and mechanical properties can be significantly altered with the WAAM conditions [14]. Huang et al. investigated the tensile behavior of as-built and machined specimens WAAMed with different deposition strategies using normal and high-strength steel, and reported that the machined samples showed almost isotropic behavior, whereas as-built samples showed considerable anisotropy [15]. In addition, they reported the effects of deposition strategy on microstructure can be different when the material composition is changed. Another study from the same institution has reported significant anisotropy of both as-built and machined WAAMed sheet tensile specimens [16]. Tonelli et al. examined the effect of active cooling on the mechanical properties of 304L stainless steel and found no significant effect of active cooling on part properties [17]. On the other hand, Laghi et al. studied the effect of surface finishing, orientation, process parameters, and cooling strategy on the mechanical properties of the steel specimens and concluded that all the investigated conditions influence the mechanical properties, and cooling strategy requires a specific investigation [18]. Taken together, the above studies and many others have shown that the influences of WAAM process parameters on output properties may vary significantly and requires detailed investigation.

One of the most important factors that changes the properties of produced parts in above studies is the experienced local thermal history and it draws significant attention in the literature. Several methods have been implemented to understand and/or control the thermal history of parts in WAAM to improve output quality. These methods include but not limited to convective heat transfer ratio enhancement by applying cold air [5, 9, 18], manufacturing the sample immersed in a cooling liquid [19, 20], thermoelectric cooling [21, 22], heat input reduction [23], or allowing the temperature drops by interlayer dwelling [9, 10, 24]. The main aim to reduce the temperature in these studies is to reduce dimensional inaccuracies and built failures. However, when an active cooling is applied, the obtained high cooling rates can be detrimental to the material [4]. Temperature control by interlayer dwelling is particularly attractive since it can be applied with no additional expensive equipment and can eliminate the issues associated with fast cooling rates. Montecchi et al. studied the interlayer dwell time scheduling via finite element analysis and demonstrated that the dimensional accuracy could be improved by controlling heat accumulation with suitable interlayer dwelling [5]. Wang et al.

showed that the interlayer dwell time and travel strategies alter the microstructure of Ti6Al4V [25]. Abusalma et al. demonstrated that the interlayer dwell time significantly affects the residual stress profile of the parts fabricated by WAAM [26]. Xiong et al. investigated the effect of interlayer temperature in WAAM of 300M steel and found that the microstructure and waviness of the parts are correlated with interlayer temperature. Singh et al. tested different interlayer dwell times on 316 L stainless steel walls created by WAAM with four layers and concluded that the interlayer dwell time affects the density, geometry, microstructure, and mechanical properties of the resulting parts [9]. Similar results were reported by Nagasai et al. on low carbon steel components with four layer height [10]. Together, mounting evidence suggests that interlayer dwelling could be a viable approach to achieving the improved output quality in WAAM. By controlling the thermal history, the microstructure, part geometry, surface quality, and mechanical properties can be improved.

Although the merits of interlayer dwelling have been shown in the previous studies, the existing studies on interlayer dwelling have limited focus in terms of investigated numbers of layers, dwell times or process outputs. A further understanding of the effect of interlayer temperature and interlayer dwelling time on the output quality of the parts manufactured with different materials by WAAM is necessary to facilitate predictable WAAM of high-quality parts. For this reason, this study employs a comprehensive investigation of the effect of interlayer dwell time on microstructural and mechanical properties of very-high-aspect-ratio low carbon low alloy steel parts manufactured by WAAM. Sixty-layer height samples were manufactured by gas metal arc welding (GMAW)-based WAAM. Temperature profiles on both substrate and interlayer were monitored. The microstructure, hardness, dimensional properties, and location dependent strength of the components produced with and without interlayer dwelling were comparatively analyzed. The presented study aims to further expand our understanding of the WAAM process for accurate and reproducible fabrication of high-quality parts.

## 2 Experimental procedure

### 2.1 Experimental setup and materials

To study the effect of atmospheric cooling times, an experimental investigation was conducted. The WAAM was performed in a robotic cell shown in Fig. 1a to produce the samples. This robotic cell includes a 6-axis robot arm (OTC DAIHEN FD-V8L) with an end effector for welding, and a synergic gas metal arc welding (GMAW) machine (GeKa-Mac, Power MIG GPS WB P500L). During WAAM, the

**Fig. 1** **a** The experimental facility used in the study. **b** The illustration of the used build strategy along with the substrate (Ts) and interlayer (Ti) measurement locations. **c** The specimen locations and configuration extracted from the printed samples for further characterization and testing

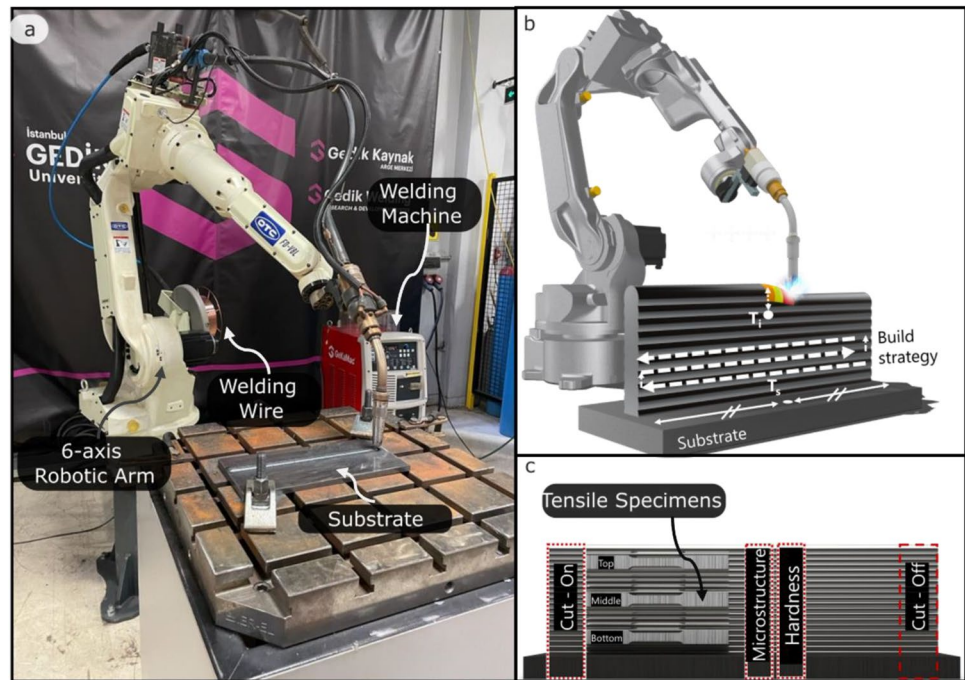


**Table 1** The composition of the used wire (SG2) and substrate material (%.wt)

Type	C	Mn	Si	P	S
<b>Welding Wire</b>	<b>0.066</b>	<b>1.462</b>	<b>0.89</b>	<b>0.005</b>	<b>0.001</b>
Substrate	0.197	1.407	0.197	0.014	0.003

The properties of used wire are emphasized with bold letters

synergistic welding machine was programmed with a low spatter control (LSC) operation to ensure short arc formation with high stability and low spatter by monitoring and adjusting voltage throughout the process. The robotic arm was controlled with teach pendants.

A commercially available low alloyed 1.2 mm AWS A5.18 ER 70 S-6 welding wire (GeKa SG2) was used in the experiments. S355J2N plain steel with the dimensions of 350 mm × 150 mm × 12 mm was used as the substrate, following the TS EN 10025-2 standard. To minimize the distortion of the substrate during the process, the substrate was clamped on the base with a torque wrench. The chemical composition of both the welding wire and the substrate material used in the experiments is given in Table 1. The WAAM process was conducted under a shielding gas consisting of 82% Ar + 18% CO<sub>2</sub> to protect the products from oxygen or nitrogen contamination.

## 2.2 Experimental plan

The samples were printed with a single bead in each layer. Due to thermal differences, the sample height could vary significantly when the same travel direction is used [9]. To

eliminate this height variation, the alternating layers were printed in opposite directions as depicted in Fig. 1b. Each sample was produced using the same tool path with 60 subsequent layers. To investigate the effect of interlayer cooling duration, three samples were produced with 0-, 60- and 120-s interlayer dwell times between successive layers. The arc was extinguished right after completing each layer and restarted for the next layer right before the movement of the robotic arm. All other experimental conditions were kept identical throughout the experiments. The samples were produced with 40 cm/min travel speed, 80 A current with a 90° torch angle, 14 mm contact tip to work distance (CTWD), and 15 L/min shielding gas flow rate. To investigate the effect of dwell times on heat accumulations, substrate and top-layer temperatures were monitored using an infrared thermometer (FLUKE 62 Mini). Since there is no standard method for measuring temperatures during WAAM, various approaches have been implemented in the literature including measuring the substrate temperatures using thermocouples or pyrometers, measuring from a constant location from the side surface, measuring from the top surface, and measuring from the side surface with a constant distance to top surface [27]. Lemes et al. compared the pyrometer measurements from top surface and side surface with a constant distance to top surface and concluded that measurement from the sideward surface represents the melt pool temperature better [28]. They also pointed out that the measured temperatures using the above approaches should be taken as reference temperatures rather than absolute temperatures. As a result, the temperatures were determined to be measured from the sideward surface. The measurement locations

and time were determined based on EN ISO 13916 which defines how the temperatures should be measured during multi-pass welding. Figure 1b shows the temperature measurement locations. The substrate temperature was measured 20 mm away from the weld bead on the mid-section of the plate, and the interlayer temperature was measured from the built wall's centerline of the manufactured wall 15 mm below the top surface. In addition, an infrared camera (FLIR E6-XT) was used to monitor the temperature distribution on the substrate and printed samples.

### 2.3 Applied tests

To determine the effect of interlayer dwell time, several dimensional, mechanical, and microstructural analyses were conducted. The porosity and crack formation in the samples were evaluated using the Digital X-Ray method according to ISO 17636-2 (DURR HD CR35). After digital X-ray analysis, specimens were extracted from the samples for further evaluation as depicted in Fig. 1c. The microstructure of the samples was investigated from the cross-sections via optical microscopy (Leica DMI8 optical microscope) after extracting cross-sectional specimens by cutting, polishing, and etching with Nital (3%) solution following by ASTM E3 standard. These cross-sections were further investigated using scanning electron microscopy (FEG, Quanta 450). The width and height of the samples were measured at least

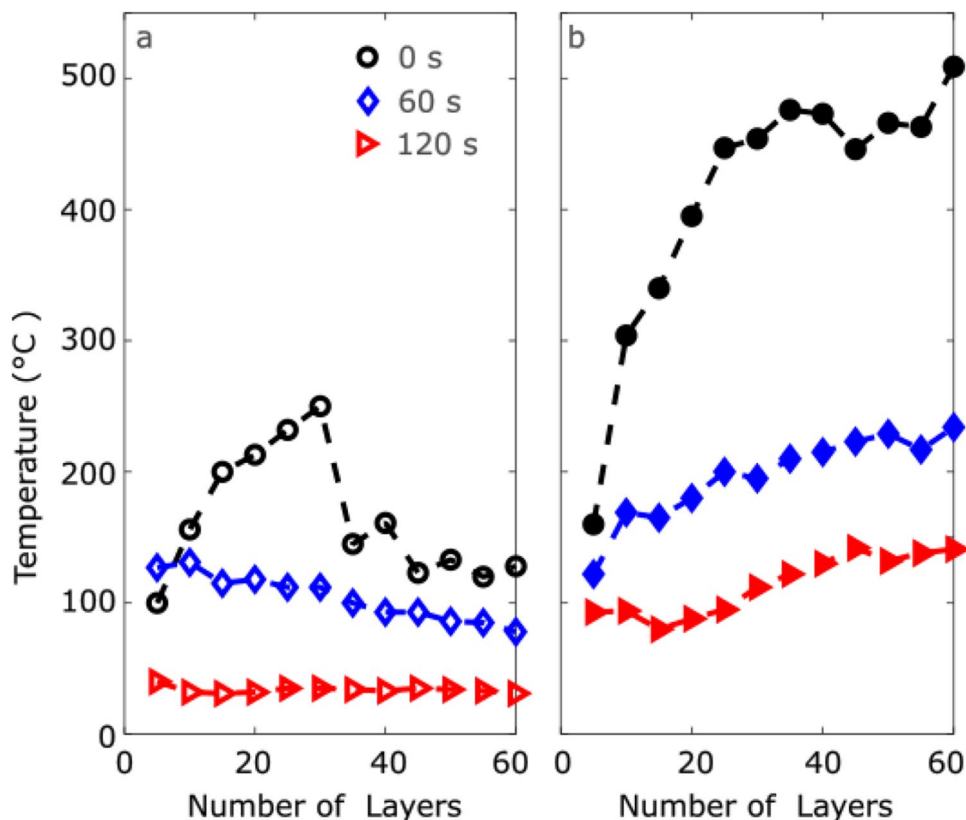
from five different locations using a caliper before sectioning the specimens. The surface waviness values were extracted from the cross-section images and extracted using image processing. In addition, the hardness variation throughout the built height was determined from the middle region of the cross-sections using a Vickers indenter with 5 kgf load (Struers DuraScan G5) based on ISO 6507 standard. The hardness measurements were taken with 0.5-mm intervals through the built height. Macro images of the samples were obtained by stitching the images obtained with a stereo microscope (NIKON SMZ 745T). To study the strength variation throughout the built height, three tensile specimens in horizontal directions were extracted from each sample based on ASTM E8/E8M-21 standard. The tensile tests were carried out on a tensile test device (Zwick Roell 600 kN) in accordance with ASTM E8/E8M-21.

## 3 Results and discussion

### 3.1 Temperature profiles and dimensional properties

Figure 2 shows the temperature values from the substrate and interlayer. The interlayer dwell time reduces substantially the temperature ranges that previous layers experience (Fig. 2a). The measured interlayer temperatures reach above

**Fig. 2** The measured temperature values from **a** the substrate and **b** interlayer at different layer levels



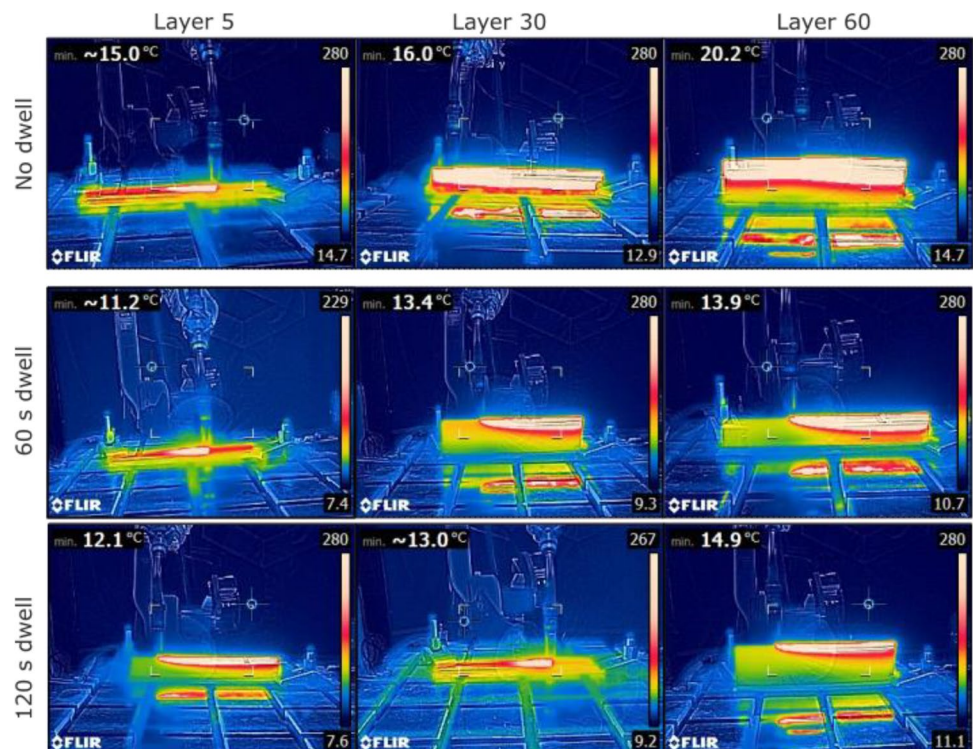
500°C without interlayer dwelling, whereas the maximum interlayer temperature with 60 s and 120 s dwelling were measured as 209°C and 142°C, respectively. The interlayer temperatures continue to increase with the built height up to approximately the 30<sup>th</sup> layer and a more steady thermal condition was observed in the successive layers in specimens without interlayer dwelling and with 60 s dwell times. On the other hand, the sample with a 120-s interlayer dwell time showed substantial reduction on both substrate and interlayer temperature. The measured substrate temperatures highlight the importance of interlayer dwelling (Fig. 2b). The substrate temperatures without dwelling continue to increase until the 30<sup>th</sup> layer reaching up to 250°C. The effect of substrate heat dissipation on the interlayer temperature is evident on the first layers, especially the sample with no interlayer dwell time showed substantial reduced heat dissipation and increased interlayer temperatures with increasing built heights. Conversely, interlayer dwelling allows the accumulated heat to dissipate, thereby decreasing the substrate and interlayer temperatures with increasing built heights. Considering the previous studies that use substrate temperature to follow the interlayer temperatures (e.g., [29, 30]), the obtained results clearly show that the substrate temperature cannot be a good reference for the interlayer temperatures even in the first layers.

Figure 3 shows the thermal field images of the samples at the 5<sup>th</sup>, 30<sup>th</sup>, and 60<sup>th</sup> layers of each sample. Although the temperature limit of the used infrared camera is only 280°C, the output thermal distributions are still very informative to

compare the thermal distribution and heat dissipation effects of the investigated interlayer dwell times. The heat accumulation increases with the increasing number of layers. Furthermore, the interlayer dwell time decreases the temperature on the already deposited layers and reduces the heat accumulation throughout the samples and the substrate. The shorter dwell times act as the preheating on the interlayer and reduce both the solidification and heat dissipation rates.

The temperature profiles affect the dimensional accuracy of the produced parts. Figure 4 shows the pictures of the produced parts along with their cross-sectional views. The cross-sectional views reveal that the first deposited layer on all the samples has the lowest width due to the fast dissipation of the heat through the substrate and lower substrate temperature. However, with the subsequent layers, the previous surfaces maintain the preheating from the earlier layer, and thus, the larger width is obtained. Table 2 shows the overall height, width, and surface roughness variations with standard deviations of the produced parts. The minimum height and the maximum width were observed in the sample with no interlayer dwelling, with height and width values of 68.46 mm and 4.81 mm, respectively. The maximum height of 73.03 mm was measured in the sample with a 120-s interlayer dwell time. The width of the samples was reduced to 4.43 mm and 4.26 mm with increasing interlayer dwell times to 60 s and 120 s, respectively. This is expected since the interlayer dwelling accelerates the dissipation of heat on the deposited surface, thereby solidifying the newly deposited layer faster, with reduced spreading. Since the volumetric

**Fig. 3** Thermal field images of the samples produced with different interlayer dwell times during 5<sup>th</sup>, 30<sup>th</sup>, and 60<sup>th</sup> layer deposition



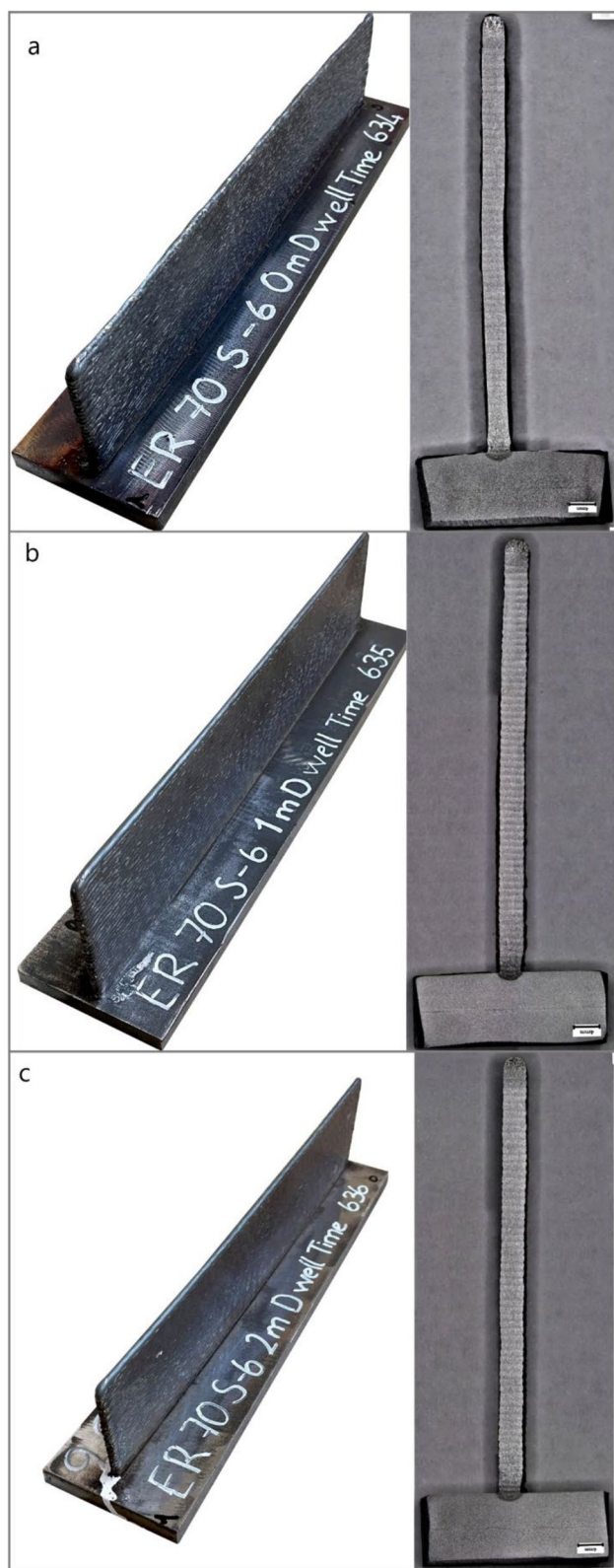


**Fig. 4** The wire arc additive manufactured components with different interlayer dwell times along with their cross-section views. **a** No interlayer dwell time, **b** 60s interlayer dwell time, **c** 120s interlayer dwell time (the scale bar on the cross-section images corresponds to 4 mm length)

**Table 2** Dimensional properties of WAAMed parts with standard deviations obtained with different interlayer dwell times

Interlayer dwell time	Height ( $\sigma$ ) (mm)	Width ( $\sigma$ ) (mm)	Average waviness ( $\mu\text{m}$ )
Continuous	68.46 ( $\pm 2.11$ )	4.81 ( $\pm 0.23$ )	298
60s	71.52 ( $\pm 0.79$ )	4.43 ( $\pm 0.1$ )	219
120s	73.03 ( $\pm 0.6$ )	4.26 ( $\pm 0.01$ )	203

rate is similar for each dwelling time, lower sample widths and higher sample heights are obtained with increasing interlayer dwell time. It should be noted that the standard deviations both in height and width decreased with increasing dwell time pointing out more uniform samples were obtained with increasing dwell time. The measured average waviness values were 298  $\mu\text{m}$ , 219  $\mu\text{m}$ , and 203  $\mu\text{m}$  for the samples with 0-s, 60-s, and 120-s interlayer dwell times, respectively. These average waviness values suggest that the increasing dwell time also imparts higher surface quality by reducing the layer-by-layer surface waviness.

### 3.2 Micro and macro defects

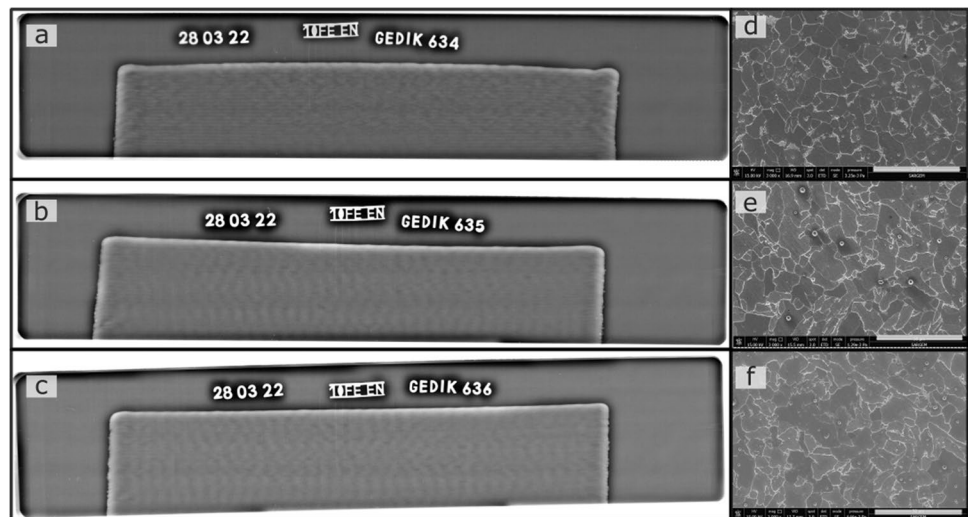
Figure 5a–c shows the digital X-ray and SEM images of the manufactured samples with different interlayer dwell times. No defects were observed with X-ray imaging analysis of all three samples, confirming the favorable experimental conditions to achieve fusion of the successive layers. In addition, these crack-free samples demonstrate the lack of major quality issues due to the thermal stress-related residual stresses.

Further characterization of the sample cross-sections with optical microscopes exhibits no microscopic defects (Fig. 6). However, the SEM images shown in Fig. 5e, f indicate that the samples contain holes with an approximate diameter of 2  $\mu\text{m}$ . A further investigation of the relationship between dwell times and these defects is warranted as a future study.

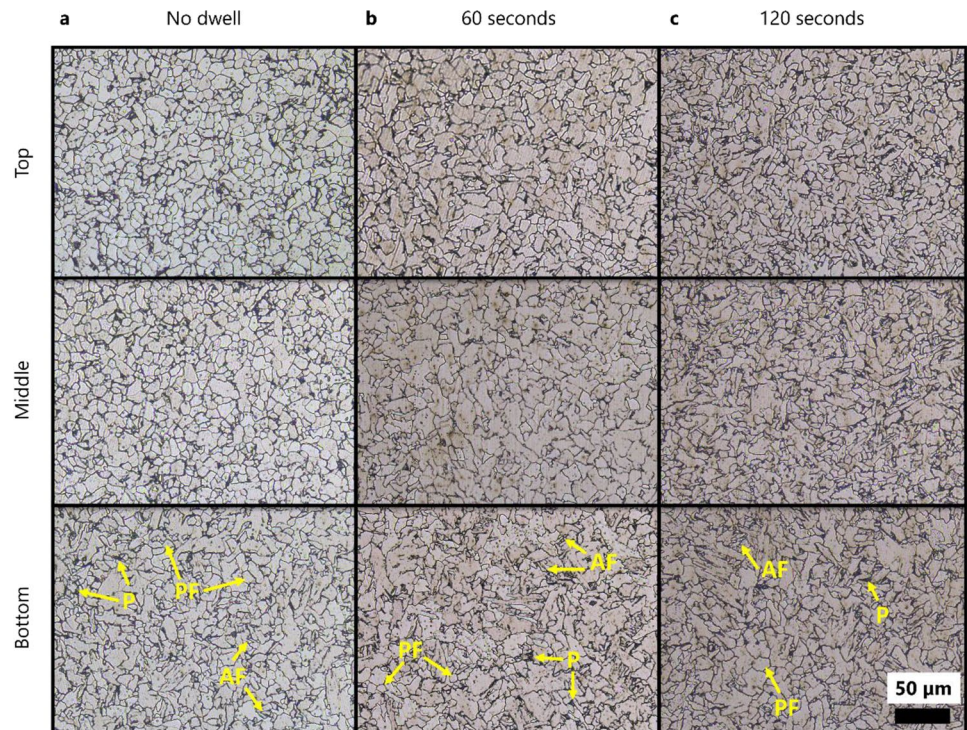
### 3.3 Microstructural developments

Figure 6 shows the microstructures obtained from the bottom (approximately 5 mm above the substrate), middle (approximately mid-height), and top regions (approximately 15 mm below the top surface) of the produced samples with different interlayer dwell times. The micrographs of the sample without interlayer dwelling revealed that the microstructure of the bottom region composed of the typical polygonal as the primary phase and a low-volume fraction of acicular ferrite and grain boundary ferrite due to the faster cooling that was mainly caused by the substrate plate (Fig. 1a). The solid wire used in WAAM is hypoeutectoid steel with a low carbon content of  $C \leq 0.07\%$  and containing increased silicon and manganese content.

**Fig. 5** Defect characterization of the samples: **a, b, c** Digital X-ray photos of the samples with 0 s, 60 s, and 120 s dwell time, respectively. **d, e, f** Scanning electron microscopy images of the sample cross-sections of specimens produced with 0 s, 60 s and 120 s dwell time, respectively. Scale bars on SEM images are 50  $\mu\text{m}$



**Figure 6:** Microstructure of the samples manufactured with interlayer dwell times. **a)** 0 s **b)** 60 s **c)** 120 s interlayer dwell times



Thus, there is a small amount of pearlite phases, which have primarily formed along the ferrite grain boundaries. However, the microstructure of the middle and top regions significantly differs from the microstructure of the bottom region. Figure 6a shows that the acicular ferrite phase in the middle and top regions decreased, and the general microstructure became a more equiaxed ferrite structure with a small amount of pearlite at the grain boundaries due to the increased interlayer temperature resulting from continuous deposition characteristics of WAAM, compared to bottom regions. Gurol et al. also reported that

heat accumulation increases in the middle and top regions with the increased building layers [31].

Since the fusion boundaries experience a higher cooling rate during the solidification process compared with continuous deposition, both parts in all regions (bottom, middle, and top) consisted of polygonal ferrite structure with a small amount of acicular ferrite structure in the samples produced with 60-s and 120-s dwell times. Further analysis of grain sizes was obtained using ImageJ. When the dwell time was increased from 60 to 120 s, the average grain sizes decreased from 16.31  $\mu\text{m}$  to 11.74  $\mu\text{m}$  in the investigated regions.

During WAAM, the heat-affected zone can reach several layers depending on the existing heat accumulation. Depending on the existing temperatures, in the reheated layers migration of grain boundaries and grain growth can occur [12]. Since the previously built layers with no dwell time and 60-s dwell times hold higher temperatures, the tendency to have recrystallized equiaxial microstructure is higher on these samples compared to the sample produced with a 120-s dwell time.

Thus, change in dwell time from 60 to 120 s resulted in an increased amount of acicular ferrite structure and the decreased grain size due to lower interlayer temperatures. Moreover, the bottom regions exhibited smaller grains compared to others due to the substrate cooling effect as described for continuous deposition as well.

### 3.4 Hardness and strength

The Vickers hardness graph of the samples manufactured with different dwell times is shown in Fig. 7. To include the changes in the transition zone, the measurements were started from the center of the substrate. The highest hardness values were found in the heat-affected zone (HAZ) regions of the substrate in all three different dwell times. The hardness values were found to be gradually decreasing with increased distance from the substrate up to about a 15-mm built height. The high hardness in the bottom regions could be a result of the fast cooling of these regions due to the fast dissipation of the heat through the thick substrate. The hardness value increases with the increase in the interlayer dwell time. The average hardness values from approximately 10 mm above from the substrate to up to a 60-mm built height were measured as 143.4, 158.2, and 168.9 HV with 4.38,

4.78, and 6.51 HV standard deviation for the samples produced with 0 s, 60 s, and 120 s dwelling, respectively. The reason for the increase in hardness with increasing dwell times can be attributed to the faster solidification and cooling rates. In all the samples, there was a gradual increase in hardness at the top layers. Indeed, in each newly deposited layer, the previous layers experience cyclic heat waves that decreases hardness. On the other hand, the top layers experience a lower number of thermal cycles, and thus, the higher hardness values were retained.

Tensile tests were carried out to determine the effect on the mechanical values of the parts produced with different dwell times. As depicted in Fig. 1c, the tensile samples were extracted from the deposited walls from three different height regions to understand the possible effect of the built height. Figure 8 shows the yield strength and elongation values of the tensile specimens. The yield strength of the samples increased with increasing interlayer dwell times predominantly due to faster cooling rates. Except for the sample produced with continuous deposition without interlayer dwelling, the highest yield strength values were measured on the specimens extracted from the bottom region. On the sample without interlayer dwelling, the increment in the yield strength, was balanced with the reduction of the strength due to the longer duration of experienced high-temperature ranges because of fast heat transfer to the substrate. Thus, no significant variation in yield strength was observed. The deviations of the yield points due to specimen location were calculated as 3.25%, 10.6%, and 4.4% respectively. The high variation of the sample with a 60-s dwell time was interpreted because of the interlayer temperature ranges. As seen in Fig. 2, with 60 s of interlayer dwelling,

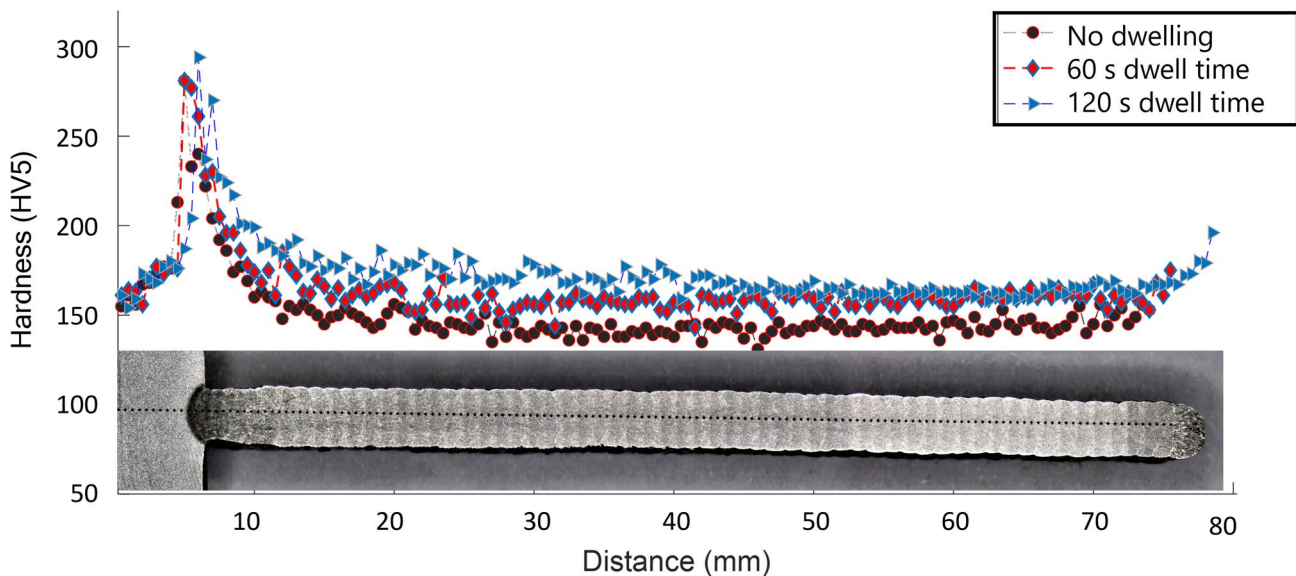
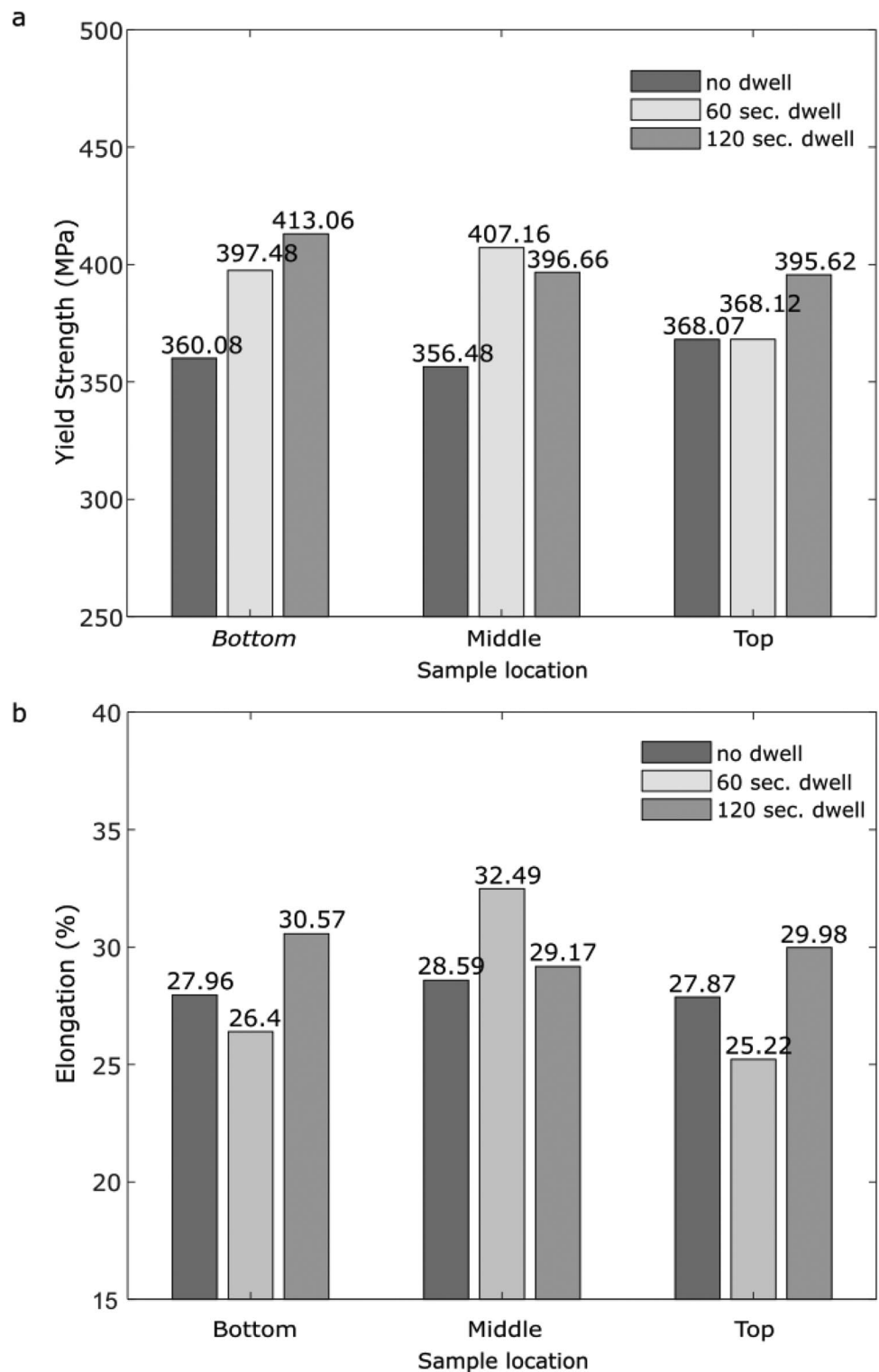


Fig. 7 Vickers hardness variation of samples produced with investigated interlayer dwell times



**Fig. 8** The tensile test results for specimens horizontally extracted from the bottom, middle, and top regions of the WAAMed samples with different interlayer dwell times. **a** Yield strength and **b** elongation



the mid-twenty-fifth layer, the interlayer temperatures were measured higher than 200°C. With increasing the number of layers, the heat accumulation increased, and consecutively the yield strength was reduced.

Further investigation of the obtained yield strengths was executed using analysis of variance (ANOVA). As

it is seen in the ANOVA results shown in Table 3, the effect of interlayer dwell time was found to be statistically significant with a *P*-value of 0.045, and the rest of the one-way and two-way interactions parameters were found to be statistically insignificant (*P*-value > 0.1). The further elaborate, mean effects plots for the yield strength were

**Table 3** Analysis of variance for the yield strength (DF: Degree of Freedom; Adj SS: Adjusted sums of squares; Adj MS : Adjusted mean squares)

Source	DF	Adj SS	Adj MS	F-value	P-value
Model	5	3030,89	606,18	2.77	0.215
Linear	2	2679,13	1339,57	6.12	0.087
Location (L)	1	250,65	250,65	1.15	0.363
Dwell time (D)	1	2428.48	2428.48	11.10	0.045
Square	2	190.09	95.04	0,43	0.683
L*L	1	18.28	18.28	0.08	0.791
D*D	1	171.80	171.80	0.79	0.441
Error	3	656.42	218.81		
Total	8	3687.31			

depicted in Fig. 9, and the increase in the yield strength with increasing dwell time was clearly observed.

The elongation of the samples did not show a clear trend; however, all the samples showed a higher elongation than the manufacturer-specified value (manufacturer's specification: min 22%). The variation of the elongation due to specimen location was calculated as 2.58%, 28.82%, and 4.79% for the specimens with 0-s, 60-s, and 120-s interlayer dwell times, respectively. ANOVA for the elongation also confirmed that all the one-way and two-way interactions were statistically insignificant.

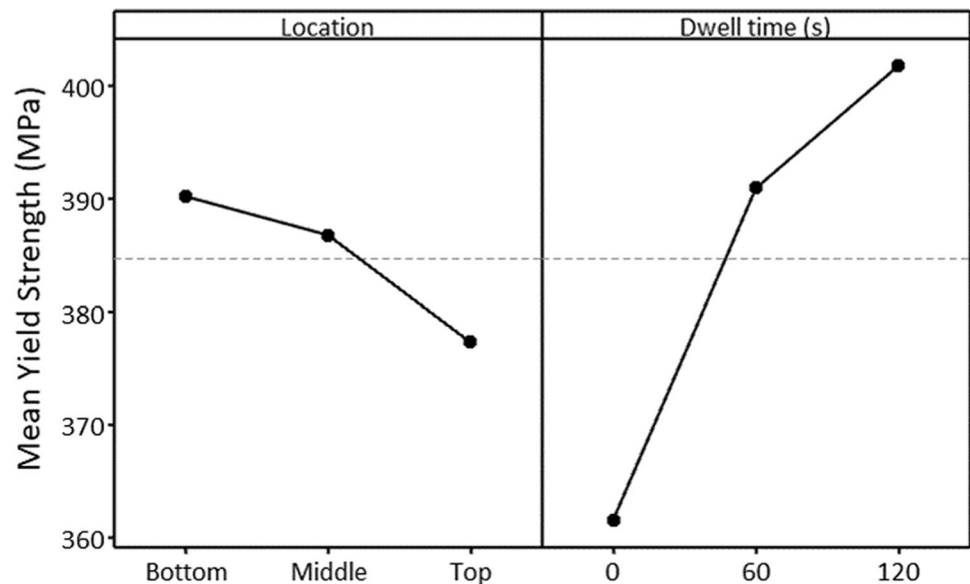
The manufacturer-specified yield point of the used ER 70 S-6 welding wire is min. 420 MPa. Although all the investigated specimens demonstrated lower stresses than the specified value, the obtained strength of the samples exhibits that the used WAAM parameters were suitable to manufacture mechanically robust parts.

## 4 Conclusions

In this study, we conducted an experimental investigation of WAAM to gain an in-depth understanding of the effect of interlayer dwell time on the process output quality. Three samples containing sixty layers were manufactured by WAAM using three different interlayer dwell conditions. The temperature of the substrate and the interlayer were measured. The microstructure, hardness, and strength properties of the produced samples were evaluated. Based on the obtained results, for the studied process parameter combinations the following conclusions are drawn:

- (i) The mechanical properties and microstructure of the samples are altered with the duration of interlayer dwelling under the investigated conditions.
- (ii) The increase in dwell time tends to improve the hardness and yield strength of the low alloyed steels due to the faster the cooling rates.
- (iii) Near the thick substrate, the generated heat dissipates faster, and the ensuing fast cooling yields elongated microstructures with high hardness values and yield points. The temperature distributions of the samples show that the effect of interlayer dwell time is not identical throughout the built height, suggesting that instead of a constant dwell time, it would be better to adjust the interlayer dwell time throughout the process according to the temperature of the depositions of the new layer.
- (iv) Since the heat conduction towards the cold regions on the sample and substrate is crucial, the sample geometry must be considered when determining a favorable interlayer dwelling condition.

**Fig. 9** Main effects plot for yield strength



**Acknowledgements** The authors thank Mrs. Hülya Kümek and the staff members of the Welding Technology Research and Development Center of the İstanbul Gedik Üniversitesi for their technical support during the preparation and characterization of the WAAM samples, and Assoc. Prof. M. F. Serincan of Gebze Technical University for his assistance in thermal camera measurements, Dr. Emrullah Korkmaz for valuable discussions.

**Funding** This work was supported by Gedik Welding INC, Turkey

## Declarations

**Competing Interests** The authors declare no competing interests.

## References

- Rodrigues TA, Duarte V, Miranda RM et al (2019) Current status and perspectives on wire and arc additive manufacturing (WAAM). *Materials (Basel)* 12. <https://doi.org/10.3390/ma12071121>
- Jafari D, Vaneker THJ, Gibson I (2021) Wire and arc additive manufacturing: opportunities and challenges to control the quality and accuracy of manufactured parts. *Mater Des* 202:109471. <https://doi.org/10.1016/j.matdes.2021.109471>
- Oliveira JP, Santos TG, Miranda RM (2020) Revisiting fundamental welding concepts to improve additive manufacturing: from theory to practice. *Prog Mater Sci* 107:100590. <https://doi.org/10.1016/j.pmatsci.2019.100590>
- Cunningham CR, Flynn JM, Shokrani A et al (2018) Invited review article: Strategies and processes for high quality wire arc additive manufacturing. *Addit Manuf* 22:672–686. <https://doi.org/10.1016/j.addma.2018.06.020>
- Montevecchi F, Venturini G, Grossi N et al (2018) Heat accumulation prevention in Wire-Arc-Additive-Manufacturing using air jet impingement. *Manuf Lett* 17:14–18. <https://doi.org/10.1016/j.mfglet.2018.06.004>
- Wu B, Ding D, Pan Z et al (2017) Effects of heat accumulation on the arc characteristics and metal transfer behavior in Wire Arc Additive Manufacturing of Ti6Al4V. *J Mater Process Technol* 250:304–312. <https://doi.org/10.1016/j.jmatprotec.2017.07.037>
- Zhao H, Zhang G, Yin Z, Wu L (2011) A 3D dynamic analysis of thermal behavior during single-pass multi-layer weld-based rapid prototyping. *J Mater Process Technol* 211:488–495. <https://doi.org/10.1016/j.jmatprotec.2010.11.002>
- Le VT, Mai DS, Hoang QH (2020) Effects of cooling conditions on the shape, microstructures, and material properties of SS308L thin walls built by wire arc additive manufacturing. *Mater Lett* 280:128580. <https://doi.org/10.1016/j.matlet.2020.128580>
- Singh S, Jinoop AN, Tarun Kumar GTA et al (2021) Effect of interlayer delay on the microstructure and mechanical properties of wire arc additive manufactured wall structures. *Materials (Basel)* 14(15):4187. <https://doi.org/10.3390/ma14154187>
- Nagasai BP, Malarvizhi S, Balasubramanian V (2022) Effect of interlayer delay on microstructure and bead geometry of wire arc additive manufactured low carbon steel components. *Int J Interact Des Manuf*:1–8. <https://doi.org/10.1007/s12008-022-01009-6>
- Wang JF, Sun QJ, Wang H et al (2016) Effect of location on microstructure and mechanical properties of additive layer manufactured Inconel 625 using gas tungsten arc welding. *Mater Sci Eng A* 676:395–405. <https://doi.org/10.1016/j.msea.2016.09.015>
- Rafieezad M, Ghaffari M, Vahedi Nemani A, Nasiri A (2019) Microstructural evolution and mechanical properties of a low-carbon low-alloy steel produced by wire arc additive manufacturing. *Int J Adv Manuf Technol* 105:2121–2134. <https://doi.org/10.1007/s00170-019-04393-8>
- Rafieezad M, Nemani AV, Ghaffari M, Nasiri A (2021) On microstructure and mechanical properties of a low-carbon low-alloy steel block fabricated by wire arc additive manufacturing. *J Mater Eng Perform* 30:4937–4945. <https://doi.org/10.1007/s11665-021-05568-9>
- Müller J, Hensel J, Dilger K (2022) Mechanical properties of wire and arc additively manufactured high-strength steel structures. *Weld World* 66:395–407. <https://doi.org/10.1007/s40194-021-01204-1>
- Huang C, Kyvelou P, Zhang R et al (2022) Mechanical testing and microstructural analysis of wire arc additively manufactured steels. *Mater Des* 216:110544. <https://doi.org/10.1016/j.matdes.2022.110544>
- Kyvelou P, Slack H, Daskalaki Mountanou D et al (2020) Mechanical and microstructural testing of wire and arc additively manufactured sheet material. *Mater Des* 192:108675. <https://doi.org/10.1016/j.matdes.2020.108675>
- Tonelli L, Sola R, Laghi V et al (2021) Influence of interlayer forced air cooling on microstructure and mechanical properties of wire arc additively manufactured 304L austenitic stainless steel. *Steel Res Int* 92(11):2100175. <https://doi.org/10.1002/srin.202100175>
- Laghi V, Palermo M, Gasparini G et al (2021) On the influence of the geometrical irregularities in the mechanical response of wire-and-arc additively manufactured planar elements. *J Constr Steel Res* 178:106490. <https://doi.org/10.1016/j.jcsr.2020.106490>
- Scotti FM, Teixeira FR, da Silva LJ, de Araujo DB, Reis RP, Scotti A (2020) Thermal management in WAAM through the CMT advanced process and an active cooling technique. *J Manuf Process* 57:23–35. <https://doi.org/10.1016/j.jmapro.2020.06.007>
- da Silva LJ, Souza DM, de Araújo DB et al (2020) Concept and validation of an active cooling technique to mitigate heat accumulation in WAAM. *Int J Adv Manuf Technol* 107:2513–2523. <https://doi.org/10.1007/s00170-020-05201-4>
- Li F, Chen S, Shi J et al (2018) Thermoelectric cooling-aided bead geometry regulation in wire and arc-based additive manufacturing of thin-walled structures. *Appl Sci* 8(2):207. <https://doi.org/10.3390/app8020207>
- Shi J, Li F, Chen S et al (2019) Effect of in-process active cooling on forming quality and efficiency of tandem GMAW-based additive manufacturing. *Int J Adv Manuf Technol* 10:349–1356. <https://doi.org/10.1007/s00170-018-2927-4>
- Rodrigues TA, Duarte V, Avila JA et al (2019) Wire and arc additive manufacturing of HSLA steel: effect of thermal cycles on microstructure and mechanical properties. *Addit Manuf* 27:440–450. <https://doi.org/10.1016/j.addma.2019.03.029>
- Montevecchi F, Venturini G, Grossi N et al (2018) Idle time selection for wire-arc additive manufacturing: a finite element-based technique. *Addit Manuf* 21:479–486. <https://doi.org/10.1016/j.addma.2018.01.007>
- Wang J, Lin X, Li J et al (2019) Effects of deposition strategies on macro/microstructure and mechanical properties of wire and arc additive manufactured Ti–6Al–4V. *Mater Sci Eng A* 754:735–749. <https://doi.org/10.1016/j.msea.2019.03.001>
- Abusalma H, Eisazadeh H, Hejrjipour F et al (2022) Parametric study of residual stress formation in wire and arc additive manufacturing. *J Manuf Process* 75:863–876. <https://doi.org/10.1016/j.jmapro.2022.01.043>
- João L, Reis RP, Scotti A (2019) The potential of IR pyrometry for monitoring interpass temperature in wire + arc additive manufacturing. *Evol Mech Eng* 3:1–4. <https://doi.org/10.31031/EME.2019.03.000553>

28. Jorge VL, Teixeira FR, Scotti A (2022) Pyrometrical interlayer temperature measurement in WAAM of thin wall: strategies, limitations and functionality. *Metals (Basel)* 12(5):765. <https://doi.org/10.3390/met12050765>
29. Denlinger ER, Heigel JC, Michaleris P, Palmer TA (2015) Effect of inter-layer dwell time on distortion and residual stress in additive manufacturing of titanium and nickel alloys. *J Mater Process Tech* 215:123–131. <https://doi.org/10.1016/j.jmatprotec.2014.07.030>
30. Hackenhaar W, Mazzaferro JAE, Montevecchi F, Campatelli G (2020) An experimental-numerical study of active cooling in wire arc additive manufacturing. *J Manuf Process* 52:58–65. <https://doi.org/10.1016/j.jmapro.2020.01.051>
31. Gürol U, Dilibal S, Turgut B, Koçak M (2022) Characterization of a low-alloy steel component produced with wire arc additive manufacturing process using metal-cored wire. *Mater Test* 64:755–767. <https://doi.org/10.1515/mt-2021-2155>

**Publisher's note** Springer Nature remains neutral with regard to jurisdictional claims in published maps and institutional affiliations.

Springer Nature or its licensor (e.g. a society or other partner) holds exclusive rights to this article under a publishing agreement with the author(s) or other rightsholder(s); author self-archiving of the accepted manuscript version of this article is solely governed by the terms of such publishing agreement and applicable law.